Research Square

Preprints are preliminary reports that have not undergone peer review.
They should not be considered conclusive, used to inform clinical practice,
or referenced by the media as validated information.

Endothelin B Receptor Mutant Exhibits Craniofacial Dysmorphology Resembling Domestication Syndrome

Ko-Chin Chen (ckochin@gmail.com)
Australian National University
Allison Gee
Australian National University
Geoffrey Croaker
Australian National University

Research Article

Keywords: Hirschsprung Disease, ETB mutant, craniofacial dysmorphology, Domestication Syndrome

Posted Date: July 9th, 2021

DOI: https://doi.org/10.21203/rs.3.rs-685151/v1

License: This work is licensed under a Creative Commons Attribution 4.0 International License.
Read Full License

Abstract

Background:

$ET_B^{-/-}$ mutation is a major cause of HSCR, a neurocristopathy known for its enteric nervous system failure. Other than regulating ENCC migration, ET_B mediates ET-1 clearance. Consequently, ET_B may indirectly affect ET-1/ET_A signaling, which controls CNCC migration and craniofacial development. Interestingly, it was hypothesized that “domestication syndrome” arise from changes in neural crest determining genes, including ET_A and ET_B. While $ET_A^{-/-}$ animals are known to suffer severe dysmorphology resembling CATCH22 syndrome, we hypothesize that *sl/sl* rat, an $ET_B^{-/-}$ HSCR model animal, may exhibit subtle craniofacial changes through indirect control. These features may share resemblance to those of domestication syndrome.

Methods:

Ten rat pups with an average age of 88 hours were anaesthetized with 5% isoflurane and culled via exsanguination. Tail tips were removed for genotyping. Head tissue were stained in 1.5% iodine for two weeks prior to micro-CT scanning. *In vivo* micro-CT scanning of cranial specimen was performed followed by *ex vivo* micro-CT scanning of 2 samples for image quality control. 3D visualization and analyses were performed using open-source program, Drishti. Cephalometric measurements were made based on selected craniofacial landmarks. Comparisons were made between *sl/sl* rats and the control group, which consisted of wild-type and heterozygotes.

Results:

Subtle reductions in facial measurements were seen in *sl/sl* rats when compared with the control group, ranging from 1.4% to 15%. These changes were observed in cranial, maxillary and mandibular parameters: total skull length, nasal length, nasal width, nasal cavity width, interorbital width, interlens distance, inner and outer canthal distance, maximal skull height, cranial length, intracranial length and width, interorbital width, and interzygomatic width. Consistently, craniofacial ratio indices showed *sl/sl* rat has a flatter cranium (skull height/skull length: 0.393 vs 0.413) and a shorter but broader nose (nasal-width/nasal-length: 0.794 vs 0.874). Additionally, subtle dystopia canthorum may be presented in *sl/sl* rat based on increased W index. While there was no discrepancy in dental number and morphology between the control and *sl/sl* groups, dimensional difference was detected.

Conclusions:

This study demonstrated subtle craniofacial changes are presented in $ET_B^{-/-}$ HSCR model, supporting the idea that ET_B regulates CNCC migration. The findings also implicate HSCR patient may have predisposing risks for conditions such as obstructive sleep apnea, cleft palate, or dental malocclusion. Lastly, these changes share resemblance with described domestication syndrome, supporting NCC-determining gene, ET_B, may play a role in the formation of domestication.

Background

Colonic aganglionosis are diseases affecting both humans and animals, with Hirschsprung disease (HSCR) being the human eponym. While HSCR was once thought of as a single-organ disease, it has become apparent that as a neurocristopathy, multi-systems are likely involved. Indeed, a number of congenital abnormalities of the central nervous system including microcephaly, agenesis of the corpus callosum, asymmetry of lateral ventricles, central hypoventilation syndrome, sensorineural deafness, seizures, mental retardation and autonomic nervous abnormalities have all been reported to associate with HSCR (1–5). Additionally, it is widely accepted that HSCR is associated with a number of genetic syndromes including Shah-Waardenburg syndrome (WS-IV), Down's syndrome (DS), and Mowat-Wilson syndrome (MWS) (6). Furthermore, we also recorded smaller head circumference in pediatric surgical patients with HSCR than those of general pediatric surgical population. This observation was more pronounced in males, consistent with HSCR's male predominance (7). These evidence suggest that developmental failure in HSCR is not limited to, at least in some cases, the enteric nervous system but more diffusely affecting central nervous, cardiovascular, and craniofacial systems, as exemplified by MWS. In this study, we focus on the external morphological changes associated with HSCR phenotype.

Several genes have been identified in the pathogenesis of HSCR. A major susceptible gene is *RET*, which contributes 5–25% of all cases based on the findings of genetic screening series (8). Additionally, the endothelin signaling pathway also plays important role in the pathogenesis of HSCR; mutations in either endothelin B receptor (ET_B) or endothelin-3 (ET-3) genes can lead to HSCR, as identified in both HSCR patients and rat models (9, 10). ET_B is the second most susceptible gene for causing HSCR, accounting for approximately 5% of human cases (8). The loss-of-ET_B-function results in WS-IV and other developmental sequelae due to the signaling disruptions in the endothelin system.

Endothelin signaling is an intricate system, encompassing two major endothelin receptors, ET_A and ET_B. Their respective signaling pathways have distinctive different yet intertwined physiological functions. While a functional ET_B is known to play pivotal role in the development of ENS, it also mediates basal endothelial vasodilation and up to 80% of ET-1 clearance; the latter of which is less well-known (11). Binding of ET-1 and ET_A mediates strong vasoconstriction through vascular smooth muscle contractions, and importantly, is essential for the craniofacial morphogenesis during development. Indeed, Clouthier et al (1998) demonstrated mice with ET_A knock-out mutations exhibit features resembling human CATCH 22 or velocardiofacial syndrome, including: smaller mandible, shortened neck, underdeveloped pinnae, and deformed cardiovascular outflow tracts (12).

Bony and cartilaginous craniofacial morphogenesis are heavily dependent on three major stages of CNCC developments: migration of CNCC from rhombomere to pharyngeal arches forming the ectomesenchymal cells, propagation of ectomesenchymal cells within the pharyngeal arches, and terminal differentiation to mature structures (e.g. cartilage, dentine, and bones) following interactions with ectoderm (13). While the precise mechanisms of ET-1/ET_A signaling on the developing CNCC have yet to be confirmed, the current consensus is as follows: ET-1 expressed in the pharyngeal arch epithelium

and paraxial mesoderm-derived arch core acts as a chemoattractant for the ET_A-expressing ectomesenchymal cells to appropriate position prior to end-organ differentiation (12). Therefore, disruptions or hypostimulations in ET-1/ECE-1/ET_A pathway leads to CNCC migration failure and severe craniofacial defects ultimately result in mechanical asphyxia post birth (12, 14, 15). Additionally, the ectomesenchymal cells originated from cardiac neural crest cells (CaNCC) migrate to pharyngeal arches 3, 4, and 6 to form the aortic pulmonary system; disruptions in the ET-1/ET_A system can thus cause ventricular septal defects and aortic hypoplasia or interruptions (14).

Interestingly, the multi-genetic “domestication syndrome” also exhibits mild variant craniofacial dysmorphology seen in velocardiofacial syndrome and Waardenburg syndrome (WS); both of which arise from mutations in the endothelin system (16, 17). Domestication syndrome was a concept first introduced by Charles Darwin in 1868 to describe a range of behavioral, morphological and physiological traits difference between the domesticated animals and their wild forbearers (18). Since then, the genetics and implications of this have been the focus of extensive researches (19). The domestication syndrome refers to a combination of traits observed in domesticated animals including increased docility, tameness and prolonged juvenile behavior, depigmentation, ear and tail form, shorter nose, reduced tooth size, alterations in adrenocorticotropic hormone levels, altered concentrations of several neurotransmitters, and a reduction in total brain size and particular brain regions (19–21). Many of the similar characteristics are also observed in HSCR-associated syndromes, suggesting potential common etiology. Indeed, recent researches have suggested that features of domestication may arise from alterations in neural crest cells and neural crest determining genes, including RET, GDNF, SOX10, MITF, PAX3, ET-1, ET-3, ET_A, and ET_B genes, all of which play crucial roles in neural crest cell specification, migration, and post-migratory interaction (10, 22–28). Consistently, animals with these dysfunctional genes may display a range of abnormalities, ranging from mild domestication syndrome to debilitating or lethal neurocristopathy such as HSCR or Waardenburg syndromes (19, 27).

Although we do not expect ET_B-knockout mutants to exhibit gross dysmorphic features from the migration failure of cephalic neural crest cell (CNCC) as seen in ET-1/ET_A mutants, we ponder the potential impact of elevated ET-1 on the development of HSCR subjects. To study the potential changes associated with HSCR, we adopted spotting-lethal (*sl/sl*) rat as our study model.

sl/sl rat is an autosomal recessive $ET_B^{-/-}$ mutant with high adherence to Mendelian inheritance. Pathogenically, *sl/sl* rat carries a naturally-occurring 301 base-pair deletions in ET_B gene resulting ET-3/ET_B signaling dysfunction (9). Phenotypically, *sl/sl* rat exhibits features resembling HSCR and WS-IV patients including: histologically-confirmed aganglionic bowel, pigmentation defects, and hearing deficits (9, 29). Based on the colony data of 475 rats, we observed high genetic penetrance of intestinal aganglionosis in up to 95% of homozygous *sl/sl* rats. Additionally, Gariepy et al (2000) showed *sl/sl* rats having approximately six-times higher ET-1 level than that of wild-type rats due to impaired clearance from the absence of functional ET_B (30). This was also supported by the consistent finding that ET_B inhibition by BQ-788 caused significant elevation of ET-1 levels (31). Consequently, we suspect potential

developmental changes in craniofacial features to occur in *sl/sl* rats due to elevated ET-1 levels and subsequent changes in ET_A-mediated signaling.

Given *sl/sl* rat is a single-gene HSCR model with high genetic penetrance, changes observed in mutants can provide further clarifications to the ET_B functions and potential impairments associated with HSCR. In addition to skin depigmentation, we ponder *sl/sl* rats may display similar characteristics of domestications, including craniofacial changes.

This study aims to extrapolate the impact of ET_B on the craniofacial morphology by quantitatively comparing the external morphology of *sl/sl* rat to that of control group. All measurements are made on three-dimensional (3-D) rendering of structurally preserved micro-CT data. We hypothesized that *sl/sl* rats may possess altered craniofacial morphology resembling domestication features, including smaller a shorter and flatter face.

Methods

2.1. Compliance with Ethical practice

All animal tissues used in this study were handled with strict compliance to ACT Health Human Research Ethics Committee (ACTH-HREC) and Australian National University Animal Experimentation Ethics Committee (ANU-AEEC), project number A2011/67. Additionally, this report is reported in accordance with ARRIVE guidelines.

2.2. Tissue preparation and staining.

Ten rat pups with an average age of 88 hours were used this study. They were derived from the crossbreeding between the heterozygous carriers of the ET_B mutation. Their coat pattern, age, gender, weight, and colonic appearance were recorded prior to culling. The culling process involved over-anesthetizing the rats with 5% isoflurane followed by thoracotomy and abdominal aortomy. Five-millimeter tail tips of each rat were resected and stored for subsequent genotyping.

To facilitate successful micro-CT scanning with adequate tissue differentiation, diffusion staining with iodine solution was performed prior to scanning. A rhomboid-shaped craniotomy of five-millimeter in diameter was created on parietal bones to facilitate tissue staining. The rat samples were first washed in 10% PBS solution for 30 minutes followed by 4% formalin fixation for 24 hours. Next, formalin was replaced by progressive ethanol (EtOH) series: 20%, 50%, 70% and 90% for 24 hours each to replace the formalin. Finally, the ethanol-fixed rat bodies were stained in 1.5% iodine solution for a minimum of 7 days prior to micro-CT scanning (32).

2.3. Micro-CT Scanning

We have chosen micro-CT scanning for its high image-resolution power to secure accurate and detailed anatomical information. The image scanning was performed using a commercially available *in vivo*

micro-CT scanner (Caliper Quantum FX) followed by a validation scan with a custom-built *ex vivo* micro-CT system at the Department of Applied Mathematics of Australian National University (ANU). Due to its limited accesses, the latter was only used for image quality control. The terminology of "*in vivo*" and "*ex vivo*" described here are not to be confused with their standard definitions in biomedical science but rather as descriptions of micro-CT system setups (29). The *in vivo* micro-CT system consists of a stationary sample positioned in between a rotational system of X-ray source and detector with the aim to reduce radiation exposure while acquiring satisfactory images. On the contrary, the *ex vivo* micro-CT system positions a rotating sample in between an adjustable X-ray source and a detector for maximal magnification and image data with the high signal-to-noise ratios.

The Caliper Quantum FX required a scanning time of 4.5 minutes for images with maximal resolutions of 10 μm/voxel. The resultant images were stored as DICOM series. On the other hand, the *ex vivo* micro-CT system of ANU Applied Mathematical Department allocated 15 hours of scanning time per scan with additional 8 hours of image-processing time via National Computational Infrastructure (NCI) services. The maximal resolution achievable was 1 μm/voxel, limited by the physical size of the sample. The resultant images were stored as netCDF files. Both series of image formats were visualized and analyzed using Drishti, an open-source software (33).

2.4. Genotyping

Following the cephalometric analysis on acquired micro-CT data, genotyping was completed by standard PCR protocols. Three homozygous wild-type ($ET_B^{+/+}$), two heterozygotes ($ET_B^{+/-}$), and five homozygous spotting-lethal (*sl/sl*; genotype $ET_B^{-/-}$) rats were identified.

Genotyping was performed with following protocols. Cells of the isolated five-millimeter rat-tail segments were lysed using Proteinase K in lysis buffer, which consisted of 100mM Tris pH 8, 5mM EDTA, 0.2% SDS, 200mM NaCl in distilled water. DNAs were extracted via standard protocols: vortex heating, supernatant separation via centrifuging, and washing and drying DNA pellet with 70% EtOH. The extracted DNA was quantified with spectrophotometry.

Next, PCR was completed using "Master-Mix" reagents composed of 10*PCR buffer, Qiagen-contained $MgCl_2$, dNTP (10mM), Primer PS 7 (33.3μM, 5'-CCACTAAGACCTCCTGGACT-3'), Primer PS 15 (33.3μM, 5'-AGTGTAGCTTTCTAAGTCGTGA-3') and DNA polymerase (34). The Mater-Mix reagents were pipetted onto PCR plates with 13 DNA samples, including the 3 controls ($ET_B^{+/+}$, $ET_B^{+/-}$ and $ET_B^{-/-}$). PCR was conducted in the Veriti 96-Well Thermal-Cycler. Finally, the DNA identification against the controls was performed by running electrophoresis at 100V and 55mA with molecular-weight ladder (MassRuler, #SM1263, Fermentas) for one hour. The electrophoresis gel was visualized with Gel Documentation System DOC-PrintVX5 (Vilber Lourmat).

2.5. Cephalometric Analysis

A selection of cranial, maxillary, mandibular, and dental structures were chosen for analysis. The anatomical landmarks in this study were made based on anthropometric and cephalometric references in previous studies (35–38). These descriptions were outlined in Fig. 1 and Table 1. Based on these craniofacial landmarks, direct dimensional measurements, as outlined in Fig. 2 and Table 2, were completed using Drishti (33).

Table 1: Description of cephalometric landmarks selected for dimensional analysis.

*: refers to labelling shown in **Figure 1**; (): same landmarks visualized in different planes.

Table 2: Description of cephalometric measurements.

	Cephalometric Point	Description
Surface Cranial Cephalometric Points		
1	Internasal Point	The most anterior point of the internasal suture in the mid sagittal plane
2	Nasofrontal point	Intersection of the nasofrontal suture and the internasal suture on the midsagittal plane
3	Frontoparietal Point	The intersection of the frontoparietal suture and the interparietal suture on the midsagittal plane
4	Occipital point 1	The most posterior point on the external occipital crest
5	Lateral Nasal Point	The most lateral point of the external snout
6	Inner canthal point	The most medial point of the margin on the eyelid
7	Outer canthal point	The most lateral point of the margin of the eyelid
8	Orbital Point	The most superior and medial point of the orbit
9	Tympanic point	The most inferior point of the tympanic process in the midsagittal plane.
Axial Cranial Cephalometric Points		
10	Posterior Nasal Spine 1	The most posterior point of the posterior nasal spine on an axial slice taken at the point of maximal lens protrusion
11	Occipital point 2	The most posterior point on the occipital bone, measured in the axial plane
12	Internal Nasal Point	The most lateral point of the nasal cavity
13	External lens point	The post lateral point of the lens
14	Temporal point	The most lateral point on the temporal bone from the midsagittal plane
15	Superior orbital point	The most superior point of the orbit
16	Lateral Orbit point	The most lateral point of the orbit
17	Inferior Orbit point	The most inferior point of the orbit
Maxillary Cephalometric Points		
18	Incisive foramen lateral point	The most lateral point of the incisive foramen
19	Key ridge point	Most lateral point of the maxilla at the join of the maxilla and zygoma

20	U6 mesial point	most anterior point of the U6 molar
21	Zygomatic point	The most lateral and inferior point of the zygomatic arc
22	U8 distal point	most posterior point of the U8 molar
23	Posterior Nasal Spine 2	The most posterior point of the posterior nasal spine on an axial slice at the midpoint of the philtrum
Dental Cephalometric Points		
24	Inferior incisor, inferior point	The most superior tip of the inferior incisor
25	Inferior incisor, superior point	The most posterior point of the inferior incisor.
26	Superior incisor, inferior point	The most posterior point of the superior incisor.
27	Superior incisor, superior point	The most inferior tip of the superior incisor
Mandibular Cephalometric Points		
28	Condylion point	The most posterior and superior point on the mandibular condyle
29	Gonion point	The most posterior point of the spinalis of the bony contour of the conial angle of the mandible
30	Gnathion	Lowest angle of mandible
31	Mandibular alveolar point	The deepest point on the upper part of the mandibular alveolar crest between the lower incisor and the first lower molar.
32	Menthon point	The most inferior point of the mandibular ramus
33	Inferior incisive alveolar point	The most inferior edge point on the vestibular marginal alveolar bone of the lower incisor

Number*	Measurement	Description
Surface Cranial Cephalometric Measurements		
1	Total skull length	Distance between the occipital point (4) and internasal point (1)
2	Surface Cranial Length	Distance between the occipital point (4) and nasofrontal point (2) following the curvature of the skull.
3	Surface Nasal Length	Distance between the nasofrontal point (2) and internasal point (1)
4	External Nasal Width	Distance between the two lateral nasal points (5)
5	Inner inter-canthal distance	Distance between the inner canthal points (6)
6	External interorbital width	Distance between the two orbital points (8)
7	Outer inter-canthal distance	Distance between the outer canthal points (7)
Sagittal Cranial Cephalometric Measurements		
8	Maximum skull height	Distance between the tympanic point (9) and the frontoparietal point (3)
Axial Cranial Cephalometric Measurements		
9	Axial Skull length	Distance between the occipital point 2 (11) and the internasal point (1)
10	Axial Intracranial Length	Distance between occipital point 2 (11) and posterior nasal spine point (10)
11	Nasal cavity Length	Distance between the posterior nasal spine (10) and the intranasal point (1)
12	Nasal cavity Width	Distance between the two internal nasal points (12)
13	Interlens distance	Distance between the two external lens points (13)
14	Intracranial width	Distance between the two temporal points (14)
15	Orbit length	Distance between the superior orbital point (15) and the inferior orbital points (17)
16	Orbit Width	Distance between the occipital point (8) and the lateral occipital point

		(16).
17	Orbit Circumference	Distance measured between the superior, lateral, inferior and medial orbit points, following the border of the orbit.
Maxillary Cephalometric Measures		
18	Maxillary Length	Distance between the posterior nasal spine 2 point (23) and the internasal point (1)
19	Maxillary width	Distance between the two key ridge points (19)
20	Incisive foramen width	Distance between the two lateral incisive foramen points (18)
21	U6 width	Distance between the two U6 mesial points
22	Interzygomatic width	Distance between the two zygomatic points (21)
23	U8 width	Distance between the U8 distal points (22)
24	intermolar length	Distance between the U8 distal point (22) and the U6 mesial point (21)
Dental Cephalometric Measurements		
25	Superior Incisor length	Distance between the superior incisor superior point (27) and superior incisor inferior point (26), following the curve of the incisor
26	Inferior incisor length	Distance between the inferior incisor superior point (25) and inferior incisor inferior point (24), following the curve of the incisor
Mandibular Cephalometric Measurements		
27	Ramus height	Distance between the Condylion point (28) and the gnathion point (30)
28	Mandibular Length	Distance between the condylion point (28) and the inferior incisive alveolar point (33)
29	Corpus Height	Distance between the menthon point (32) and the mandibular alveolar point (31)
30	Corpus length	Distance between the gnathion point (30) and the inferior incisive alveolar point (33)
31	Mandibular plane angle	The angle at the gnathion point (30) bounded by the Gonion point (29) and the inferior incisive alveolar point (31)

*: refers to numbers listed in **Figure 2**.

(): bracketed numbers in the measurement description refer to anatomical landmarks described in **Table 1** and **Figure 1**.

Cephalometric points were identified in several cross-sectional planes. Surface measurements were obtained from the external morphology of the rat head. Maximal skull height and incisor measurements were taken in the midsagittal plane while mandibular measurements were taken in the parasagittal plane passing through the buccal mucosa. Axial and maxillary measurements were obtained in the para-axial planes where the points of maximal lens protrusion and the midpoint of the philtrum were found, respectively. Based on these direct measurements, a selection of ratio indices was calculated to assess the proportional changes in the craniofacial features. These indices include W index, nasal length/skull length ratio, nasal width/nasal length ratio, intracranial width/intracranial length ratio, skull height/skull length ratio, maxillary width/maxillary length ratio, mandibular length/skull length ratio, mandibular corpus-height/mandibular corpus-length ratio, and mandibular ramus/mandibular length ratio.

ET_B mutation has been known to associate with WS-II and WS-IVa (39). A key clinical characteristic of WS-I is the presence of dystopia canthorum (16). To assess the presence of this phenotypic feature, the W formula, as defined for human WS, was applied (Eq. 1) to model animal measurements. As the eyelids of the neonatal rats were still fused, lens distance was used as a substitute for papillary distance.

Equation 1: W index for Dystopia Canthorum

$$W = X + Y + \frac{a}{b}$$

Where X= (2a-0.2119c-3.909)/c; Y= (2a-0.22479b-3.909)/b

(a is the internal intercanthal distance, b is the interpupillary distance, and c is the external intercanthal distance) (40).

2.6. Statistical Analysis

A total of ten rats were included in analysis and divided into a control and *sl/sl* group. The control group was composed of two wild-type ($ET_B^{+/+}$) and three heterozygous ($ET_B^{+/-}$) rat pups and five spotting lethal ($ET_B^{-/-}$) rats. Data was assessed for normality and Student's t test was applied for comparison between the control and mutant groups. A result was considered statistically significant at $p\text{-value} \leq 0.05$. Analysis was conducted using SPSS software.

2.7. Measures of statistical error

To ensure validity of the study, researchers undertaking measurements were blinded to the genotype of rats until finalization of data analysis. To ensure accuracy and reproducibility, all measurements were repeated by the same researcher two weeks after the initial analysis. The difference between the two measures was determined with random error calculation, Dahlberg's error (36, 41). The Dahlberg statistic reported the average amount of disparity between the measurement sessions.

$$D = \sqrt{\frac{\sum d^2}{2N}}$$

Where d is the difference between replicate measures and N is the number of cases.

Results

The basic parameters of the rat pups were listed in Table 3. Control and *sl/sl* groups have respective average body-weights of 13.16 ± 0.81g and 11.40 ± 1.62g, *p-value* = 0.063, translating to a difference of 13%. There was a positive correlation between body-weight and the cephalometric measurements, with the control group generally having larger craniofacial measures than those of *sl/sl* rats, apart from average inferior incisor length, Tables 4 and 5. In addition to this positive correlation, *sl/sl* rat exhibited several morphological features different from the control group, as revealed by dimensional-ratio index, Table 6.

Table 3: Basic characteristics of study population.

Rat	Genotype	Rat number (n)	Average Weight (g)
Control group	$ET_B^{+/+}$ & $ET_B^{+/-}$	5	13.1552
sl/sl	$ET_B^{-/-}$	5	11.4029

Table 4: Detectable morphological difference between the control ($ET_B^{+/+}$ and $ET_B^{+/-}$) and *sl/sl* ($ET_B^{-/-}$) rats.

Craniofacial measurement	Control		Spotting-lethal		Spotting-lethal/Control Ratio	Dahlberg error*	Student's t test
	Mean (mm)	Sd (mm)	Mean (mm)	Sd (mm)			
Surface measurements							
Surface skull length	23.318	0.554	22.778	1.276	98.23%	0.210	0.411
Surface nasal length	10.062	0.395	8.729	0.849	86.75%	0.859	0.013
Surface nasal width	7.994	0.275	7.625	0.470	95.38%	0.649	0.168
Surface Interorbital width	5.735	0.515	5.331	0.553	92.96%	0.587	0.266
Inner canthal distance	8.365	0.243	8.248	0.125	98.60%	0.109	0.414
Outer canthal distance	12.191	0.585	11.749	0.404	96.37%	0.255	0.242
Sagittal Measurements							
Maximal skull height	11.887	0.458	11.567	0.276	97.31%	0.339	0.217
Axial Measurements							
Axial skull length	22.21	0.819	21.391	0.379	96.31%	0.419	0.77
Intracranial length	12.424	0.648	11.959	0.469	96.25%	0.429	0.23
Intracranial width	11.134	0.265	10.756	0.397	96.60%	0.580	0.114
Nasal cavity length	9.786	0.297	9.432	0.340	96.38%	0.278	0.118
Nasal cavity width	5.713	0.346	5.464	0.309	95.64%	0.239	0.265
Axial interorbital width	3.696	0.105	3.543	0.263	95.86%	0.278	0.262
Interzygomatic width	12.244	0.344	11.583	0.577	94.60%	0.318	0.059

* Dahlberg errors were given for standalone measurements. Errors were unable to be calculated for averaged data.

Table 5: Orbital and maxillary-facial reductions were associated with *sl/sl* rats.

Maxillary-facial measurement	Control		Spotting-lethal		Spotting-lethal/ Control	Dahlberg error*	Student's t test
	Mean (mm)	Sd (mm)	Mean (mm)	Sd (mm)	Ratio		
Orbital Measurements							
Interlens distance	10.873	0.439	10.14	0.303	93.26%	0.101	0.015
Average orbit length	3.715	0.063	3.64	0.116	97.99%	-	0.244
Average orbit width	3.325	0.153	3.324	0.157	99.97%	-	0.992
Average orbit circumference	11.012	0.309	10.668	0.359	96.88%	-	0.143
Maxillary Measurements							
Maxillary length	11.007	0.540	10.506	0.557	95.45%	0.350	0.187
Maxillary width	6.444	0.496	6.113	0.272	94.86%	0.552	0.227
Incisive foramen width	2.031	0.114	1.941	0.061	95.57%	0.083	0.159
U6 intermolar width	5.886	0.076	5.624	0.105	95.55%	0.155	0.002
U8 intermolar width	6.186	0.167	5.851	0.152	94.58%	0.235	0.011
Average molar plate length	4.847	0.180	4.582	0.169	94.55%	-	0.044
Mandibular Measurements							
Average mandibular length	10.581	0.114	10.354	0.347	97.85%	-	0.202
Average ramus height	4.392	0.129	4.264	0.214	97.09%	-	0.286
Average corpus length	9.503	0.246	9.343	0.242	98.31%	-	0.329
Average corpus height	1.514	0.129	1.483	0.135	97.92%	-	0.716
Average mandibular plane angle	99.6	5.897	97.106	3.521	97.50%	-	0.440
Dentition Measurements							
Average superior incisor length	2.762	0.299	2.463	0.204	89.17%	-	0.102
Average inferior	4.131	0.299	4.383	0.276	106.11%	-	0.203

incisor length		
Dentition Number	**Control**	**Spotting-lethal**
Average no superior molar	6	6
Average no inferior molar	6	6

Table 6: Craniofacial dimensional indices showed *sl/sl* rats having a flatter cranium with a shorter but wider muzzle.

Organ dimensional ratio	Control	Spotting lethal	Spotting-lethal/ Control *100%
Intracranial-width/intracranial-length (axial)	0.896	0.899	100.36%
Skull-height/Skull-length (sagittal)	0.413	0.393	95.23%
Nasal-length/Skull-length (surface)	0.357	0.315	88.31%
Nasal-width/Nasal-length (surface)	0.794	0.874	109.95%
Maxillary-width/Maxillary-length	0.315	0.317	100.74%
Mandibular-length/Skull-length	0.375	0.373	99.61%
Mandibular corpus height/Mandibular-length	0.160	0.159	99.60%
Mandibular ramus/Mandibular-length	0.415	0.412	99.21%
W index	3.245	3.328	102.56%

3.1. Cranial Measures

Fifteen craniofacial dimensions were taken in the surface, parasagittal, and axial planes to assess cranial structures, as reported in Table 4. The control rats have detectably larger, ranging from 1.5–14%, cranial dimensions than *sl/sl* rats in the following parameters: total skull length, nasal length, nasal width, nasal cavity width, interorbital width, interlens distance, inner and outer canthal distance, maximal skull height, cranial length, intracranial length and width, interorbital width, and interzygomatic width. While statistically significance was only found in the respective comparison of external nasal lengths and interlens distance between two groups, the trend of *sl/sl* having smaller features has been persistent across all findings measured in various planes.

3.2. Orbital Measures

Seven measures were taken to assess the orbital size and positioning in the context of the face, Table 5. Orbital dimensions were taken from both eyes followed by averaging these findings for comparison. While the control rats exhibited larger orbits than the *sl/sl* rats in terms of length, width, and circumference, these differences were small, ranging from 0.03 to 3.12%. On the other hand, statistical significantly shorter interlens distance was noted in the *sl/sl* rats, 6.74% smaller with *p-value* = 0.015, suggesting medial displacement of the lens.

3.3. Maxillary measures

Six measures were made to assess changes in maxillary structure associated with *sl/sl* mutants. Maxillary dimensions of *sl/sl* rats group were 4.53–5.45% smaller than the control group, Table 5. This was reflected by the measurements of maxillary length, maxillary width and incisive foramen width, albeit statistical significance was not achieved. On the other hand, statistically significant size-reductions associated with *sl/sl* rat were seen in U6 intermolar width, U8 intermolar width, and molar plate length. These observations suggested *sl/sl* rats having a smaller mouth and a narrower mid-face in comparison to the control group.

3.4. Mandibular measures

To assess the lower facial changes associated with ET_B mutation, five mandibular measures were compared, including mandibular length, ramus height, corpus length, and corpus height, Table 5. While these measurements showed a general trend of subtle size-reduction in *sl/sl* rats, ranging from 1.69–2.91%, none of these measures reached statistical significance. Furthermore, comparison of mandibular plane angle showed little difference between the control and *sl/sl* groups. These findings suggested ET_B mutation may have little impact on mandibular development.

3.5. Dental measures

Because dental development is dependent on CNCC migration, a process partially regulated by ET_B signaling, dentitions of *sl/sl* rat were examined. As shown by Table 5, there was no discrepancy in terms of dentition number between the control and *sl/sl* groups. Additionally, we detected no difference in dental morphology between the two groups. On the other hand, the superior incisor length of *sl/sl* mutant was 10.83% smaller than the control rat while the opposite trend was true for inferior incisor length, 6.11% larger. While these findings did not reach strict statistical significance, *p-value* < 0.05, they were consistent with the change patterns observed in the maxillary and mandibular measurements.

3.6. Comparison of Craniofacial indices

Ratio indices were calculated to determine the dimensional proportionality of individual craniofacial features.

Cranial dimensional ratios were first compared, as shown by Table 6. While there was no difference in the intracranial-width/intracranial-length ratio between the control and *sl/sl* groups, the latter has smaller skull height/skull length ratio, indicating the presence of a flatter head. Additionally, comparisons made

on the indices of nasal length/skull length and nasal width/nasal length indices demonstrated a disproportionally shorter but wider nose in *sl/sl* rat. Furthermore, while the absolute maxillary and mandibular measurements were smaller in *sl/sl* group, its respective dimensional indices were similar to those of control group, Table 6, suggesting proportional changes.

Lastly, the W index was used to assess for the presence of dystopia canthorum, a major clinical sign of WS, occurring in up to 98% of WS-I. The W index of *sl/sl* rat was found to be greater than that of control group, 3.328 versus 3.245 with *p-value* = 0.017, Table 6.

Discussion

HSCR has traditionally been regarded as a single-organ disease despite multi-genetic involvement. ET_B mutation is one of the major causes for HSCR. While ET_B is known to exert direct control on ENCC migration through ET-3/ET_B signaling, we found dysfunctional ET_B can also lead to subtle craniofacial changes with resemblance to those of "domestication syndrome." These similarities include depigmentation, a flatter head, a shorter but broader nose, and smaller teeth (19). Our finding therefore supports the long-held hypothesis that genetic alterations in the development of NCCs contribute, at least partially, to the formation of domestication syndrome (19). The culprit, in this instance, is the ET_B mutation.

In this study, we reported craniofacial changes found in *sl/sl* rat, an autosomal recessive $ET_B^{-/-}$ HSCR model with high genetic penetrance. While there was no direct signaling linkage between ET_B and the development of CNCC documented in current literature, we found *sl/sl* rats exhibit reduced cranial, nasal, maxillary, and mandibular dimensions. As shown by Tables 4 and 5, *sl/sl* rat exhibited a smaller midface, a narrowed and shortened molar bed, a shortened muzzle, and a flattened cranium when comparing to those of the control group. Albeit small, ranging from 5–15%, these observed changes in conjunction with previously described depigmentation and reduced adrenal size (Lopez Dee, unpublished data) of *sl/sl* rat support the notion that ET_B may act as a mediator for domestication syndrome.

Additionally, dental changes resembling domestication were observed in *sl/sl* rats. Indeed, the incisor size was different between the *sl/sl* and control rats; superior incisor length was ~ 10% smaller whereas inferior incisor length was ~ 6% larger in the *sl/sl* rats. Although this observation was not fully consistent with the domestication features of global dental-size reduction, this variance may be explained by the young age of studied rats, 3.5 days. As rat's dental eruption occurs at eight to ten days postnatally and maturates between forty to fifty days post-birth (42, 43), the full dental features of domestication may not be appreciated prior to the maturation age. Nevertheless, given the domestication feature is influenced by a combination of genetic and behavioral factors, our finding on *sl/sl* rat supports the notion that ET_B can be a predisposing gene for dental changes. On the other hand, the presence of normal dental anatomy and molar teeth number in each quadrant by both the control and *sl/sl* groups suggest ET_B's impact may be small. While individual molar dimensions were not measured, size-reductions in maxillary molar plate

and mandible were seen in *sl/sl* rats, Table 5. This decreased molar bed may predispose matured *sl/sl* rat to have decreased molar size and increased risks of molar overcrowding, features consistent with domestication. Overall, our findings support ET_B likely plays a modulating role in craniofacial development.

Craniofacial morphogenesis is known to be dictated by ET-1/ET_A signaling, and hypostimulation of which leads to premature arrest of CNCC migration. This severe craniofacial dysmorphology seen in CATCH 22 or velocardiofacial syndrome results in mechanical asphyxia and early death (12). Although the subtle changes identified in *sl/sl* rats were not as drastic, they nevertheless provided supporting evidence that HSCR children may suffer subtle craniofacial maldevelopment. These facial feature changes not only may affect patients aesthetically, such as cleft-palate (44), but more importantly increases the health risks. These risks include development of obstructive sleep apnea or chronic sinusitis due to a shorter but wider nose in addition to dysphagia from a smaller oral orifice; all of which can impair children's growth. Furthermore, our findings are consistent with the notion that ET_B mediates the endocytic degradation of ET-1 and thereby indirectly affecting ET-1/ET_A signaling. As reported by Gariepy et al (2000), *sl/sl* rat has ~ 6-folds higher ET-1 due to impaired clearance (30). This likely hyperstimulates ET_A pathway, as demonstrated by the increased vascular tone in ET_B-deficient mice (45). Consequently, modulation rather than premature arrest of CNCC migration were likely to have led to the subtle craniofacial changes.

Moreover, ET_B mutation is known to associate with WS, particularly in the pathogenesis of WS-II and WS-IV (46). WS is a group of sensorineural and pigmentary disorders that are subcategorized into four subtypes based on distinctive phenotypes: dystopia canthorum (WS-I), upper limb deformity (WS-III), and HSCR (WS-IV). WS-II, on the other hand, does not have any additional symptom (47). While dystopia canthorum was previously reported in PAX3-induced WS-I, we found increased W index in the $ET_B^{-/-}$ WS-IV model with respect to the control group, 3.245 vs 3.328, *p-value* = 0.017. Although this statistically significant change is small, in conjunction with other changes observed, it raises the possibility of overlapping control between PAX3 and ET_B on the CNCC migration. On the other hand, other than the nasal dimensional indices showing distinctive shorter but wider nose in *sl/sl* rat, the dimensional ratio indices made on cranium, maxilla, and mandible showed little difference between *sl/sl* and control groups, Table 6. These proportional reductions in facial features associated with *sl/sl* rats suggests ET_B mutation exerts global inhibition on cephalic growth.

It is worth noting that the control group has larger body-size than *sl/sl* rats at culling despite similar age group, suggesting malnutrition from dysfunctional enteric system may contributes to the craniofacial difference observed. While this positive body-weight and cranial size is consistent with report made by Miller and German (1999) (48), it fails to explain the presence of non-uniform dimensional-ratio indices, Table 6. This suggests an additional independent factor is likely to have contributed to the formation of flatter cranium and shorter muzzle in *sl/sl* rats.

The findings of this study, if translatable to human HSCR patients, have several clinical implications for patient management. A genome-wide association study has recently identified ET_B gene as a major susceptibility locus for craniofacial microcephaly (49), a fact that is consistent with the craniofacial alterations observed in the *sl/sl* rat. In addition to those described in syndromic HSCR (DS, MWS, and Goldberg-Shprintzen syndrome), additional craniofacial anomalies have also been reported in non-syndromic HSCR patients, including cleft palate, broad nasal root, microcephaly, and hypertelorism (6, 50–55). Our dimensional finding supports these reports with quantitative measures. Of the craniofacial alterations identified in the *sl/sl* rat, shorter but broader nose, smaller mid-face, and decreased length of the molar bed suggested HSCR patients may be predispose to obstructive sleep apnea and dental malocclusion (56); both of which instigate with adverse health outcomes and require intervention. Additionally, we may find HSCR patients with higher risks of clinical midfacial hypoplasia based on animal findings.

We acknowledge the power of this study can benefit from a larger sample size. Nevertheless, the presence of multiple craniofacial alterations in *sl/sl* rats cannot be overlooked. Additionally, while potential dose-dependent response of ET_B was not assessed, this set-up was compliant with the autosomal recessive mendelian traits of *sl/sl* rat. Furthermore, the tissue-preparation and imaging protocols used in this study may be applicable to other model studies. Future research should aim to include a larger sample-size and corresponding morphological study on clinical HSCR patients.

Conclusion

Overall, this study demonstrated subtle craniofacial changes are presented in HSCR model and provided some support for the hypothesis of neural crest gene involvement in domestication. ET_B may be one of these genes. It also contributed to the growing body of literature suggesting manifestations of HSCR are not limited to the enteric nervous system and may extend to include craniofacial malformations that increase risks for obstructive sleep apnea, cleft palate, or dental malocclusion. Confirmatory clinical studies are therefore warranted.

Declarations

Ethical approval and consent to participate

All animals This research project was approved by both Australian Capital Territory Health Human Research Ethics Committee (ACTH-HREC) and Australian National University Animal Experimentation Ethics Committee (ANU-AEEC), project number A2011/67.

Consent to publish

Not applicable.

Availability of data and materials

All original rat micro-CT files are stored in the Canberra data centre of National Computational Infrastructure (NCI) Australia for security and processing. Original image files are available upon request. Request may be sent directly to corresponding author at ckochin@gmail.com.

Competing interests

The authors declare that they have no competing interests.

Funding

None declared.

Author's contributions

Conceived the study: KC, AG, GDH. Developed the methodology, performed the experiment and analysis: KC. Performed the image analysis and statistical data analysis: KC, AG. Wrote the paper: KC, AG. All authors have read and approved the final manuscript.

Acknowledgements

The authors gratefully acknowledge the staff of Australian National University Applied Mathematic Department for their technical support of this project.

Acknowledgements:

We would like to thank the staff of Applied Mathematic Department of Australian National University for their support of this project.

References

1. Cheng W, Au DK, Knowles CH, Anand P, Tam PK. Hirschsprung's disease: a more generalised neuropathy? Journal of pediatric surgery. 2001;36(2):296-300.

2. Croaker GDH, Shi E, Simpson E, Cartmill T, Cass DT. Congenital central hypoventilation syndrome and Hirschsprung's disease. Archives of Disease in Childhood. 1998;78(4):316-22.

3. Mowat DR, Croaker GD, Cass DT, Kerr BA, Chaitow J, Ades LC, et al. Hirschsprung disease, microcephaly, mental retardation, and characteristic facial features: delineation of a new syndrome and identification of a locus at chromosome 2q22-q23. J Med Genet. 1998;35(8):617-23.

4. Sayed M, al-Alaiyan S. Agenesis of corpus callosum, hypertrophic pyloric stenosis and Hirschsprung disease: coincidence or common etiology? Neuropediatrics. 1996;27(4):204-6.

5. Staiano A, Santoro L, De Marco R, Miele E, Fiorillo F, Auricchio A, et al. Autonomic dysfunction in children with Hirschsprung's disease. Dig Dis Sci. 1999;44(5):960-5.

6. Amiel J, Sproat-Emison E, Garcia-Barcelo M, Lantieri F, Burzynski G, Borrego S, et al. Hirschsprung disease, associated syndromes and genetics: a review. J Med Genet. 2008;45(1):1-14.

7. Goldberg EL. An epidemiological study of Hirschsprung's disease. International journal of epidemiology. 1984;13(4):479-85.

8. Croaker GDH. A Cook's tour around Hirschsprung's disease. Current Paediatrics. 2006;16(3):182-91.

9. Gariepy CE, Cass DT, Yanagisawa M. Null mutation of endothelin receptor type B gene in spotting lethal rats causes aganglionic megacolon and white coat color. Proc Natl Acad Sci U S A. 1996;93(2):867-72.

10. Puffenberger EG, Hosoda K, Washington SS, Nakao K, deWit D, Yanagisawa M, et al. A missense mutation of the endothelin-B receptor gene in multigenic Hirschsprung's disease. Cell. 1994;79(7):1257-66.

11. Fukuroda T, Fujikawa T, Ozaki S, Ishikawa K, Yano M, Nishikibe M. Clearance of circulating endothelin-1 by ETB receptors in rats. Biochemical and biophysical research communications. 1994;199(3):1461-5.

12. Clouthier DE, Hosoda K, Richardson JA, Williams SC, Yanagisawa H, Kuwaki T, et al. Cranial and cardiac neural crest defects in endothelin-A receptor-deficient mice. Development (Cambridge, England). 1998;125(5):813-24.

13. Kontges G, Lumsden A. Rhombencephalic neural crest segmentation is preserved throughout craniofacial ontogeny. Development (Cambridge, England). 1996;122(10):3229-42.

14. Kurihara Y, Kurihara H, Oda H, Maemura K, Nagai R, Ishikawa T, et al. Aortic arch malformations and ventricular septal defect in mice deficient in endothelin-1. The Journal of clinical investigation. 1995;96(1):293-300.

15. Yanagisawa H, Yanagisawa M, Kapur RP, Richardson JA, Williams SC, Clouthier DE, et al. Dual genetic pathways of endothelin-mediated intercellular signaling revealed by targeted disruption of endothelin converting enzyme-1 gene. Development (Cambridge, England). 1998;125(5):825-36.

16. Milunsky JM. Waardenburg Syndrome Type I. In: Adam MP, Ardinger HH, Pagon RA, Wallace SE, Bean LJH, Stephens K, et al., editors. GeneReviews((R)). Seattle (WA): University of Washington, Seattle University of Washington, Seattle. GeneReviews is a registered trademark of the University of Washington, Seattle. All rights reserved.; 1993.

17. Waardenburg PJ. A new syndrome combining developmental anomalies of the eyelids, eyebrows and nose root with pigmentary defects of the iris and head hair and with congenital deafness. American journal of human genetics. 1951;3(3):195-253.

18. On the 150(th) Anniversary of Darwin's Submission of One of his "Five Great Books", The Variation of Animals and Plants Under Domestication, to his publisher John Murray. Alzheimers Dement.

2016;12(1):1.

19. Wilkins AS, Wrangham RW, Fitch WT. The “Domestication Syndrome” in Mammals: A Unified Explanation Based on Neural Crest Cell Behavior and Genetics. Genetics. 2014;197(3):795-808.

20. Clutton-Brock J, Clutton-Brock J, Natural History Museum (London England). A natural history of domesticated mammals. 2nd ed. Cambridge, U.K. ; New York, NY, USA London ;: Cambridge University Press ; Natural History Museum; 1999. viii, 238 p. p.

21. Zeuner FE. A history of domesticated animals. New York,: Harper & Row; 1963. 560 p.

22. Kurihara Y, Kurihara H, Suzuki H, Kodama T, Maemura K, Nagai R, et al. Elevated blood pressure and craniofacial abnormalities in mice deficient in endothelin-1. Nature. 1994;368(6473):703-10.

23. Tassabehji M, Newton VE, Read AP. Waardenburg syndrome type 2 caused by mutations in the human microphthalmia (MITF) gene. Nat Genet. 1994;8(3):251-5.

24. Xu D, Emoto N, Giaid A, Slaughter C, Kaw S, deWit D, et al. ECE-1: a membrane-bound metalloprotease that catalyzes the proteolytic activation of big endothelin-1. Cell. 1994;78(3):473-85.

25. Edery P, Attie T, Amiel J, Pelet A, Eng C, Hofstra RM, et al. Mutation of the endothelin-3 gene in the Waardenburg-Hirschsprung disease (Shah-Waardenburg syndrome). Nat Genet. 1996;12(4):442-4.

26. Antonellis A, Bennett WR, Menheniott TR, Prasad AB, Lee-Lin SQ, Program NCS, et al. Deletion of long-range sequences at Sox10 compromises developmental expression in a mouse model of Waardenburg-Shah (WS4) syndrome. Hum Mol Genet. 2006;15(2):259-71.

27. Stanchina L, Baral V, Robert F, Pingault V, Lemort N, Pachnis V, et al. Interactions between Sox10, Edn3 and Ednrb during enteric nervous system and melanocyte development. Developmental biology. 2006;295(1):232-49.

28. Arnold S, Pelet A, Amiel J, Borrego S, Hofstra R, Tam P, et al. Interaction between a chromosome 10 RET enhancer and chromosome 21 in the Down syndrome-Hirschsprung disease association. Hum Mutat. 2009;30(5):771-5.

29. Schambach SJ, Bag S, Schilling L, Groden C, Brockmann MA. Application of micro-CT in small animal imaging. Methods. 2010;50(1):2-13.

30. Gariepy CE, Ohuchi T, Williams SC, Richardson JA, Yanagisawa M. Salt-sensitive hypertension in endothelin-B receptor-deficient rats. The Journal of clinical investigation. 2000;105(7):925-33.

31. Johnstrom P, Fryer TD, Richards HK, Harris NG, Barret O, Clark JC, et al. Positron emission tomography using 18F-labelled endothelin-1 reveals prevention of binding to cardiac receptors owing to tissue-specific clearance by ET B receptors in vivo. British journal of pharmacology. 2005;144(1):115-22.

32. Chen K-C, Arad A, Song Z-M, Croaker D. High-definition neural visualization of rodent brain using micro-CT scanning and non-local-means processing. BMC Med Imaging. 2018;18(1):38-.

33. Limaye A. Drishti, A volume exploration and Presentation Tool. Developments in X-Ray Tomography VIII; 17 October 20122012.

34. Brennan A, Dean CH, Zhang AL, Cass DT, Mirsky R, Jessen KR. Endothelins Control the Timing of Schwann Cell Generation in Vitro and in Vivo. Developmental biology. 2000;227(2):545-57.

35. Barrett RL, Harris EF. Anabolic steroids and craniofacial growth in the rat. Angle Orthod. 1993;63(4):289-98.

36. Goto S, Fujita Y, Hotta M, Sugiyama A, Maki K. Influence of differences in the hardness and calcium content of diets on the growth of craniofacial bone in rats. Angle Orthod. 2015;85(6):969-79.

37. Tsai CY, Yang LY, Chen KT, Chiu WC. The influence of masticatory hypofunction on developing rat craniofacial structure. Int J Oral Maxillofac Surg. 2010;39(6):593-8.

38. Ulgen M, Baran S, Kaya H, Karadede I. The influence of the masticatory hypofunction on the craniofacial growth and development in rats. Am J Orthod Dentofacial Orthop. 1997;111(2):189-98.

39. Issa S, Bondurand N, Faubert E, Poisson S, Lecerf L, Nitschke P, et al. EDNRB mutations cause Waardenburg syndrome type II in the heterozygous state. Hum Mutat. 2017;38(5):581-93.

40. Milunsky JM. Waardenburg Syndrome Type I. In: Pagon RA, Adam MP, Ardinger HH, Wallace SE, Amemiya A, Bean LJH, et al., editors. GeneReviews(R). Seattle (WA): University of Washington, Seattle

University of Washington, Seattle. GeneReviews is a registered trademark of the University of Washington, Seattle. All rights reserved.; 1993.

41. Kim HY. Statistical notes for clinical researchers: Evaluation of measurement error 2: Dahlberg's error, Bland-Altman method, and Kappa coefficient. Restor Dent Endod. 2013;38(3):182-5.

42. Addison WHF, Appleton JL. The structure and growth of the incisor teeth of the albino rat. Journal of Morphology. 1915;26(1):43-96.

43. Griffith JQ, Farris EJ. rat in laboratory investigation. 1949.

44. Pierpont JW, St Jacques D, Seaver LH, Erickson RP. A family with unusual Waardenburg syndrome type I (WSI), cleft lip (palate), and Hirschsprung disease is not linked to PAX 3. Clin Genet. 1995;47(3):139-43.

45. Ohuchi T, Kuwaki T, Ling GY, Dewit D, Ju KH, Onodera M, et al. Elevation of blood pressure by genetic and pharmacological disruption of the ETB receptor in mice. The American journal of physiology. 1999;276(4):R1071-7.

46. Pingault V, Ente D, Dastot-Le Moal F, Goossens M, Marlin S, Bondurand N. Review and update of mutations causing Waardenburg syndrome. Hum Mutat. 2010;31(4):391-406.

47. Tachibana M, Kobayashi Y, Matsushima Y. Mouse models for four types of Waardenburg syndrome. Pigment cell research. 2003;16(5):448-54.

48. Miller JP, German RZ. Protein Malnutrition Affects the Growth Trajectories of the Craniofacial Skeleton in Rats. The Journal of Nutrition. 1999;129(11):2061-9.

49. Zhang YB, Hu J, Zhang J, Zhou X, Li X, Gu C, et al. Genome-wide association study identifies multiple susceptibility loci for craniofacial microsomia. Nat Commun. 2016;7:10605.

50. Brunoni D, Joffe R, Farah LMS, Cunha AJB. Hirschsprung megacolon, cleft lip and palate, mental retardation and minor congenital malformations. Journal of Clinical Dysmorphology. 1983;1:20-2.

51. Goldberg RB, Shprintzen RJ. Hirschsprung megacolon and cleft palate in two sibs. J Craniofac Genet Dev Biol. 1981;1(2):185-9.

52. Hurst JA, Markiewicz M, Kumar D, Brett EM. Unknown syndrome: Hirschsprung's disease, microcephaly, and iris coloboma: a new syndrome of defective neuronal migration. J Med Genet. 1988;25(7):494-7.

53. Slavikova T, Zabojnikova L, Babala J, Varga I. An embryological point of view on associated congenital anomalies of children with Hirschsprung disease. Bratisl Lek Listy. 2015;116(11):640-7.

54. Greally MT. Shprintzen-Goldberg Syndrome. In: Adam MP, Ardinger HH, Pagon RA, Wallace SE, Bean LJH, Mefford HC, et al., editors. GeneReviews(R). Seattle (WA)1993.

55. Garavelli L, Donadio A, Zanacca C, Banchini G, Della Giustina E, Bertani G, et al. Hirschsprung disease, mental retardation, characteristic facial features, and mutation in the gene ZFHX1B (SIP1): confirmation of the Mowat-Wilson syndrome. Am J Med Genet A. 2003;116A(4):385-8.

56. Kumar AR, Steinbacher D. Advances in the Treatment of Syndromic Midface Hypoplasia Using Monobloc and Facial Bipartition Distraction Osteogenesis. Seminars in Plastic Surgery. 2014;28(4):179-83.

Figures

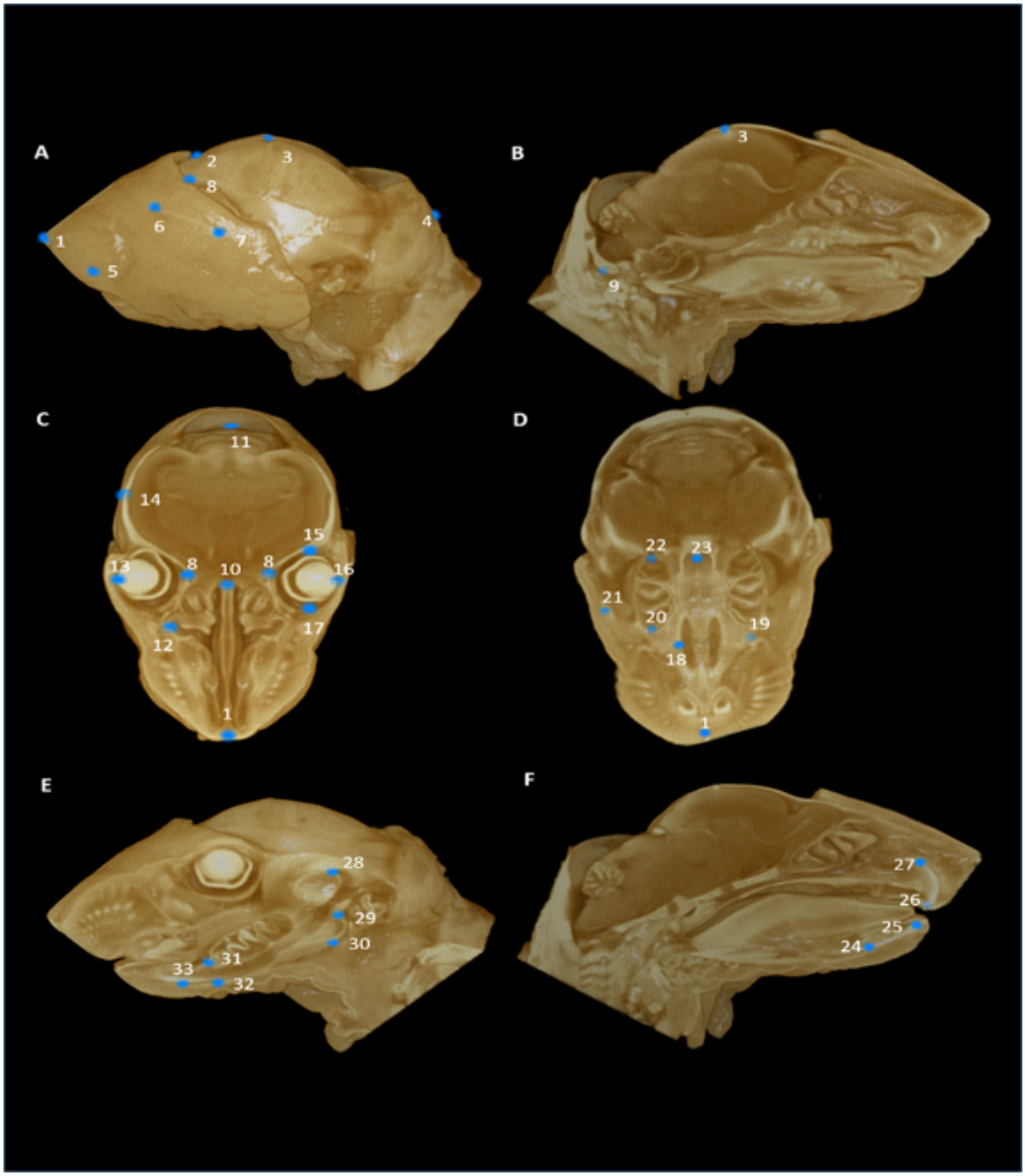

Figure 1

3-D model of rat head composed from micro-CT scans demonstrating anthropometric landmarks selected for craniofacial cephalometric analysis. A description of each numbered point is provided in Table 1. A: surface cranial cephalometric points. B: cranial cephalometric points in the mid sagittal plane. C: cranial cephalometric points in the axial plane cut at the point of maximal lens protrusion. D: maxillary cephalometric points in the axial plane cut at the midpoint of the philtrum. E: mandibular cephalometric points cut in the sagittal plane through the buccal mucosa. F: cephalometric points used to assess incisor length cut in the mid sagittal plane.

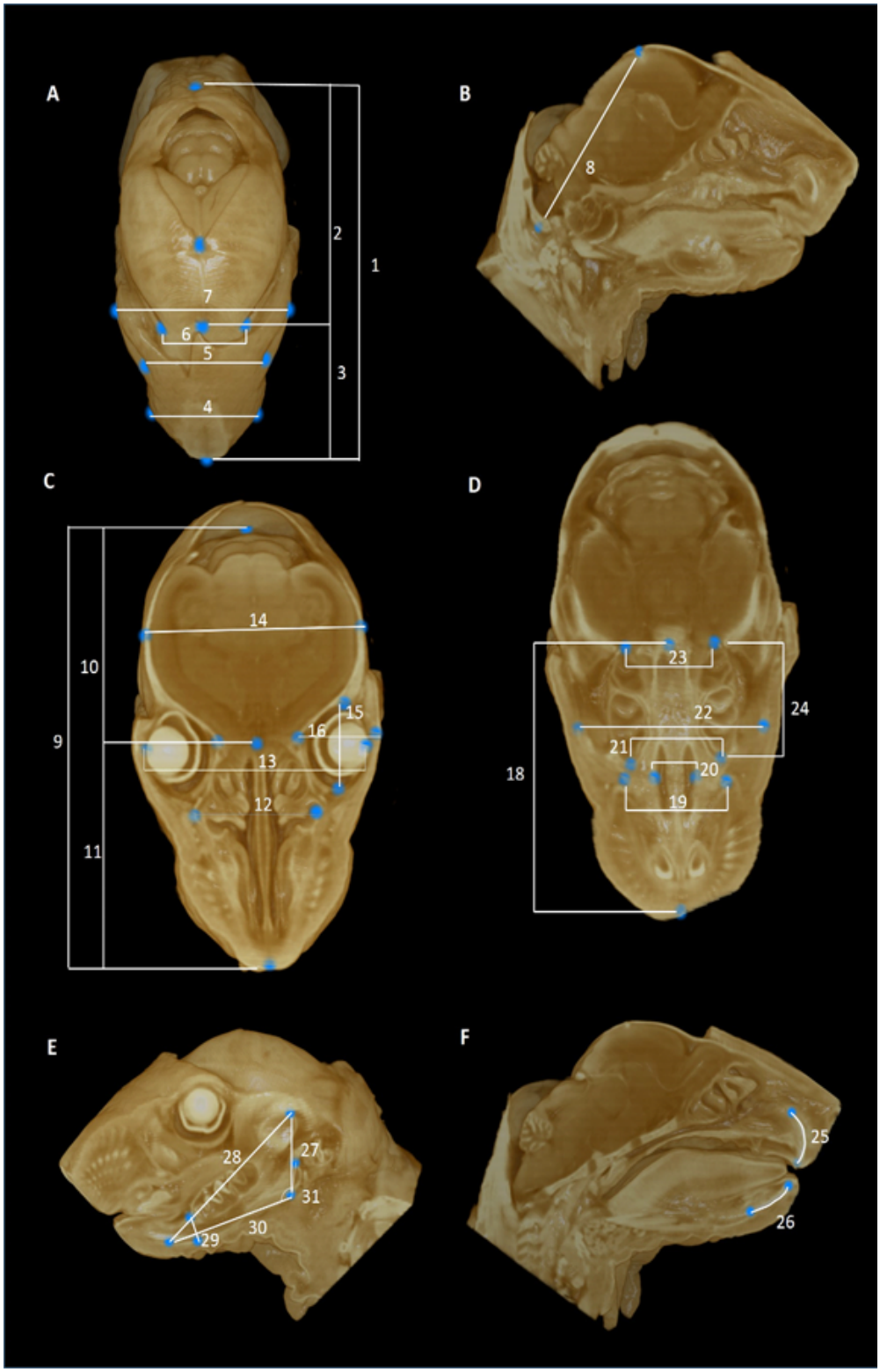

Figure 2

3-D model of rat head composed from micro-CT scans demonstrating cephalometric measurements selected for analysis. A description of each numbered point is provided in Table 2. A: Cranial cephalometric measures made from the surface of the cranium. B: Cranial cephalometric measurements made in the mid sagittal plane. C: cranial cephalometric measurements in the axial plane cut at the point of maximal lens protrusion. D: maxillary cephalometric measurements in the axial plane cut at the

midpoint of the philtrum. E: mandibular cephalometric measurements cut in the sagittal plane through the buccal mucosa. F: cephalometric measurements used to assess incisor length cut in the mid sagittal plane.

Supplementary Files

This is a list of supplementary files associated with this preprint. Click to download.

- SupplementaryTable1.docx